

# Poisson's ratio as a sensitive indicator of (fatigue) damage in fibre-reinforced plastics

W. VAN PAEPEGEM, I. DE BAERE, E. LAMKANFI and J. DEGRIECK

*Ghent University, Department of Mechanical Construction and Production, Sint-Pietersnieuwstraat 41, 9000 Gent, Belgium*

*Received in final form 10 October 2006*

**ABSTRACT** Even if the extent of damage in fibre-reinforced plastics is limited, it already affects the elastic properties. Therefore, the damage initiation and propagation in composite structures is monitored very carefully. Beside the use of nondestructive testing methods (ultrasonic inspection, optical fibre sensing), the follow-up of the degradation of engineering properties such as the stiffness is a common approach. In this paper, it is investigated if the Poisson's ratio can be used as a sensitive indicator of (fatigue) damage in fibre-reinforced plastics. Static, cyclic and fatigue tests have been performed on  $[0^\circ/90^\circ]_{2s}$  glass/epoxy laminates, and axial and transverse strain were measured continuously. The evolution of the Poisson's ratio  $\nu_{xy}$  versus time and axial strain  $\varepsilon_{xx}$  is studied. It is concluded that the degradation of the Poisson's ratio can be a valuable indicator of damage, in combination with the stiffness degradation.

**Keywords** damage mechanics; fatigue; finite element analysis; polymer-matrix composites (PMCs).

## INTRODUCTION

Damage in fibre-reinforced composites can take many forms:<sup>1,2</sup> (i) matrix cracks, (ii) fibre-matrix interface failure, (iii) fibre pull-out, (iv) delaminations and (v) fibre fracture. This damage affects the value of the elastic properties at an early stage. Especially in fatigue, the damage initiation phase can cause a pronounced drop of the elastic modulus of 5–10%. In the next damage propagation phase, the stiffness continues to decrease gradually, ranging from a few percent for unidirectionally reinforced carbon composites to several tens of percents for multidirectional glass laminates.<sup>3–7</sup>

Most one-dimensional damage models for fibre-reinforced composites only account for the effect of damage on the stiffness.<sup>8–16</sup> The degradation of the Poisson's ratio is not included in these models. Nevertheless this degradation has been observed and is not negligible.<sup>17,18</sup> Bandoh et al. showed that the Poisson's ratio of a carbon/epoxy UD laminate can drop by 50% under static tensile loading,<sup>17</sup> while Pidaparti and Vogt proved that the Poisson's ratio is a very sensitive parameter whilst monitoring fatigue damage in human bone.<sup>18</sup>

In this paper, it is investigated whether or not the Poisson's ratio can be used as a sensitive indicator of (fatigue)

damage in fibre-reinforced composites for both static, cyclic and fatigue loading. Just like the stiffness, it can be measured accurately and nondestructively. Further, it gives information about the damage state of the off-axis plies in a multi-directional composite laminate.

For long-term measurements, the use of strain gauges is less appropriate, but optical fibre sensor pads can be a viable alternative.

In a first step, static tensile tests are performed on  $[0^\circ/90^\circ]_{2s}$  glass/epoxy laminates, followed by cyclic loading-unloading tests and strain-controlled fatigue tests.

## MATERIAL AND TEST METHODS

The material under study was a glass/epoxy composite. The glass reinforcement was a unidirectional E-glass fabric (Roviglas R17/475). In the fibre direction  $\vec{e}_{11}$ , the reinforcement was 475 g/m<sup>2</sup>, while in the direction  $\vec{e}_{22}$ , the reinforcement was 17 g/m<sup>2</sup>. The epoxy matrix was Araldite LY 556.

Three stacking sequences were manufactured:  $[0^\circ]_8$ ,  $[90^\circ]_8$  and  $[0^\circ/90^\circ]_{2s}$  with the angle referred to the direction  $\vec{e}_{11}$ . The layups  $[0^\circ]_8$  and  $[90^\circ]_8$  were used for characterization in the orthotropic material directions, while  $[0^\circ/90^\circ]_{2s}$  was used for the study of the Poisson's ratio.

Correspondence: W. Van Paepegem. E-mail: Wim.VanPaepegem@UGent.be

All specimens were manufactured by vacuum assisted resin transfer moulding with a closed steel mould. The nominal thickness of all specimens was 3.0 mm and the fibre volume fraction was between 48 and 50%. The samples were cut to dimensions on a water-cooled diamond tipped saw.

The inplane elastic properties of the individual glass/epoxy lamina were determined by the dynamic modulus identification method described by Sol *et al.*<sup>19,20</sup> and are listed in Table 1.

Apart from the dynamic modulus identification method, static tensile tests on the  $[0^\circ]_8$  and  $[90^\circ]_8$  layups have been performed to check the values of the elastic properties and to determine the static strengths. It is important to mention that the mechanical behaviour in the  $\bar{e}_{11}$  and  $\bar{e}_{22}$  direction is linear until failure.

The tensile strength properties were determined from the  $[0^\circ]_8$  and  $[90^\circ]_8$  stacking sequence and are listed in Table 2.

Based on this characterization of the individual glass/epoxy lamina,  $[0^\circ/90^\circ]_{2s}$  cross-ply laminates were manufactured for investigation of the Poisson's ratio  $\nu_{xy}$ .

### STATIC MEASUREMENTS OF $\nu_{xy}$

The elastic and strength properties of the  $[0^\circ/90^\circ]_{2s}$  laminate were determined by quasi-static tensile tests on an

**Table 1** Inplane elastic properties of the individual glass/epoxy lamina

$E_{11}$ (GPa)	38.9
$E_{22}$ (GPa)	13.3
$\nu_{12}$ [-]	0.258
$G_{12}$ (GPa)	5.13

**Table 2** Tensile strength properties of the individual glass/epoxy lamina

$X_T$ (Mpa)	901.0
$\varepsilon_{11}^{ult}$ [-]	0.025
$Y_T$ (Mpa)	36.5
$\varepsilon_{22}^{ult}$ [-]	0.0025

Instron electromechanical testing machine. The tensile tests were displacement-controlled with a displacement speed of 1 mm/min.

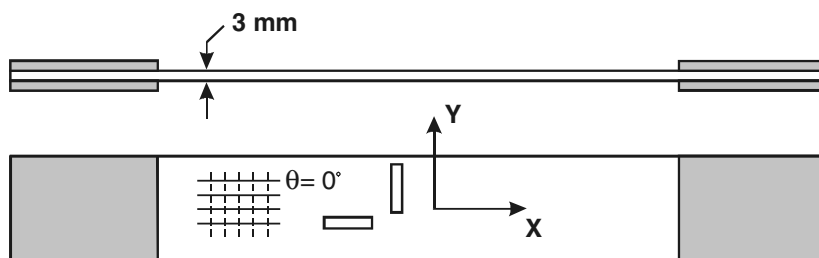
The specimen geometry is illustrated in Fig. 1. The nominal specimen width was 34 mm and the thickness 3 mm. The gauge length was 140 mm. Two strain gauges were applied in the  $X$ - and  $Y$ -direction. The tests were done in accordance with ASTM D3039 'Standard Test Method for Tensile Properties of Polymer Matrix Composite Materials'.

Figure 2 shows the stress-strain curve for the  $[0^\circ/90^\circ]_{2s}$  specimens IF4 and IF6. In the first measurement, the strain gauge signal was lost at about 1.0% longitudinal strain (due to debonding), but the load signal was measured until failure. The calculated failure stresses were 465.5 and 447.7 Mpa, respectively. The failure strain of specimen IF6 was 0.0208 (or 2.08%).

The value of the elastic modulus  $E_{xx}$  was 27.56 and 30.92 GPa, respectively (determined by least-squares linear fit for the strain range  $[0;0.0025]$ ). The value measured by the dynamic modulus identification method was 31.10 GPa for another specimen from the same batch of material.

At a level of about 100 MPa axial stress, there is a small change in slope of the stress-strain curve. The corresponding strain is slightly higher than 0.0025 (0.25%) which is the fracture strain of the  $90^\circ$  plies in the cross-ply laminate (see Table 2).

The corresponding history of the Poisson's ratio  $\nu_{xy}$  versus  $\varepsilon_{xx}$  is shown in Fig. 3. Although the axial stress-strain curve is almost linear (Fig. 2), the Poisson's ratio is decreasing quite fast. This is due to early transverse matrix cracking of the  $90^\circ$  plies. Indeed the failure strain  $\varepsilon_{22}^{ult}$  of the  $90^\circ$  plies equals only 0.0025 (see Table 2) and once the axial strain in these plies exceeds this threshold, the  $90^\circ$  plies are severely cracked. The estimated value of  $\nu_{xy}$  in the elastic regime is 0.141 and 0.152 for IF4 and IF6, respectively. The calculated value of  $\nu_{xy}$  from the dynamic modulus identification method is 0.162. The latter method is a mixed numerical/experimental method that aims to identify the engineering constants of orthotropic materials using measured resonant frequencies of freely suspended rectangular specimens. For the identification of the four orthotropic material constants, it is necessary



**Fig. 1**  $[0^\circ/90^\circ]_{2s}$  glass/epoxy specimen's layout.

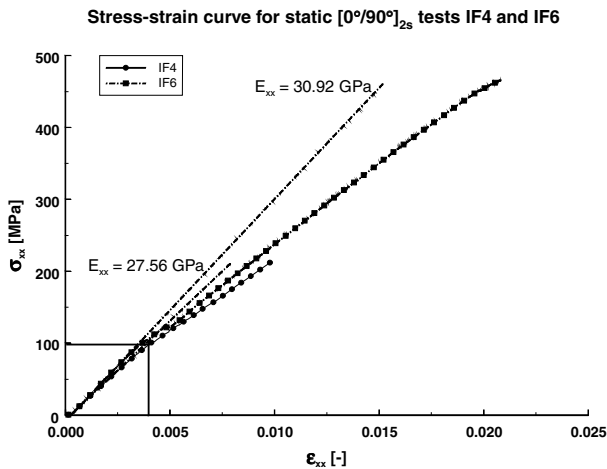


Fig. 2 Stress-strain curve for the static tensile test of the  $[0^\circ/90^\circ]_{2s}$  specimens IF4 and IF6.

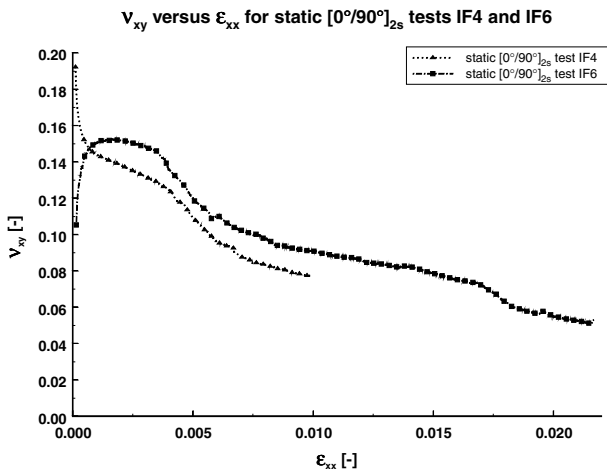


Fig. 3 Evolution of the Poisson's ratio  $\nu_{xy}$  in function of the longitudinal strain  $\epsilon_{xx}$  for the  $[0^\circ/90^\circ]_{2s}$  specimens IF4 and IF6.

to measure the first three resonant frequencies of a rectangular plate and the first resonant frequency of two beams, one cut along the longitudinal direction and the other cut along the transversal direction. Starting from an initial guess, the engineering constants are iteratively updated till a series of numerically computed resonance frequencies match the experimentally measured frequencies. This method is completely nondestructive which can explain the higher value for the Poisson's ratio.

**MEASUREMENTS OF  $\nu_{xy}$  UNDER CYCLIC LOADING**

In order to observe the behaviour of the Poisson's ratio under repeated loading, cyclic tensile tests are performed.

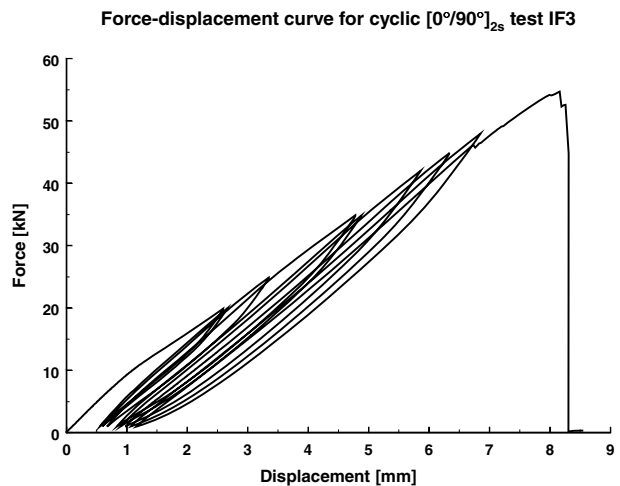


Fig. 4 Force-displacement curve for the  $[0^\circ/90^\circ]_{2s}$  specimen IF3.

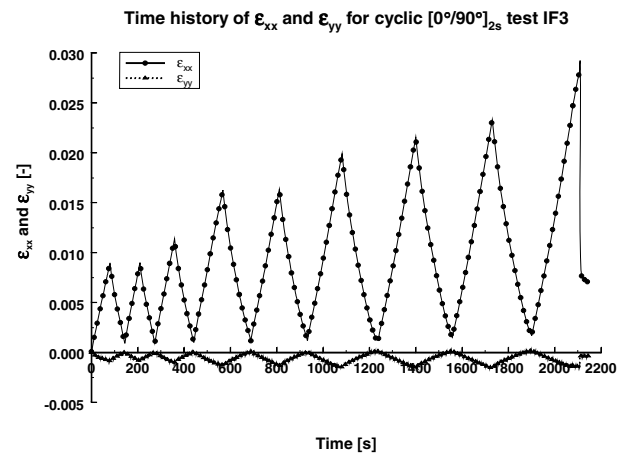


Fig. 5 Time history of  $\epsilon_{xx}$  and  $\epsilon_{yy}$  for the  $[0^\circ/90^\circ]_{2s}$  specimen IF3.

The displacement speed is 2 mm/min and the load cycles between 1 kN and subsequent load levels of 20, 20, 25, 35, 35, 42, 45, 48 and 54.7 kN (failure load), as shown in Fig. 4. The small change of the slope in the curve at 10 kN corresponds with a longitudinal stress  $\sigma_{xx}$  of 102.4 MPa. This knee-point could indeed be observed in the stress-strain curves in Fig. 2.

The corresponding time history of the measured longitudinal strain  $\epsilon_{xx}$  and the transverse strain  $\epsilon_{yy}$  for the cyclic tensile test on the  $[0^\circ/90^\circ]_{2s}$  specimen IF3 is shown in Fig. 5. At the lowest loads of 1 kN, the transverse strain  $\epsilon_{yy}$  becomes slightly positive. This is not caused by improper calibration of the strain gauges. The strain measurement channels are calibrated for each strain gauge with a precision shunt resistance. It will be shown in subsequent figures that this effect is very reproducible.

Both the failure stress and failure strain are higher than in the quasi-static tensile tests. The failure stress here is

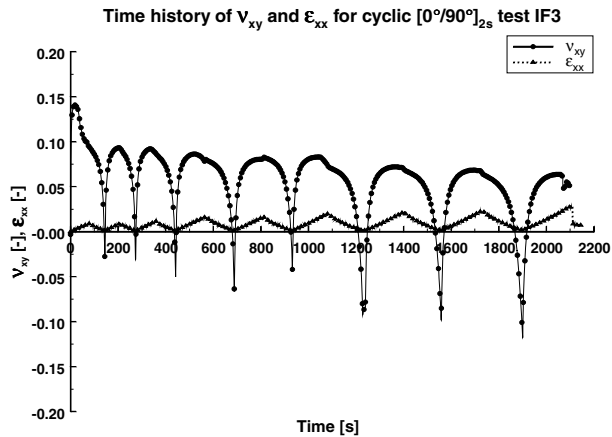


Fig. 6 Time history of the Poisson's ratio  $\nu_{xy}$  for the  $[0^\circ/90^\circ]_{2s}$  specimen IF3.

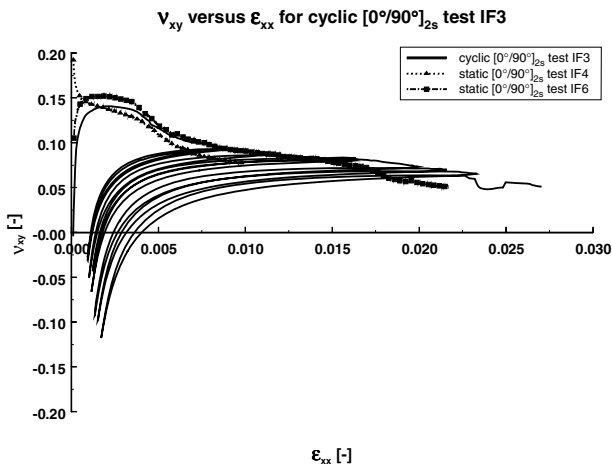


Fig. 7 Evolution of the Poisson's ratio  $\nu_{xy}$  in function of the longitudinal strain  $\epsilon_{xx}$  for the cyclic  $[0^\circ/90^\circ]_{2s}$  test IF3.

560 MPa and the failure strain 0.0293 (or 2.93%). This strengthening effect might be due to better fibre alignment. A similar phenomenon was already reported by the authors for cyclic loading/unloading tests of  $[+45/-45]_{2s}$  glass/epoxy laminates.<sup>21,22</sup>

Figure 6 shows the corresponding time history of the Poisson's ratio  $\nu_{xy}$ . In the region of low forces (and thus low strains  $\epsilon_{xx}$ ), the Poisson's ratio  $\nu_{xy}$  becomes negative, due to the slightly positive value of the transverse strain  $\epsilon_{yy}$  for small loading values (see Fig. 5).

In Fig. 7, the evolution of the Poisson's ratio  $\nu_{xy}$  is plotted against the longitudinal strain  $\epsilon_{xx}$ , together with its evolution in the quasi-static tensile tests IF4 and IF6 (see Fig. 3). It can be clearly seen that the maxima of the cyclic  $\nu_{xy}$  curves follow the static curve very well. As the Poisson's ratio changes drastically during unloading, its

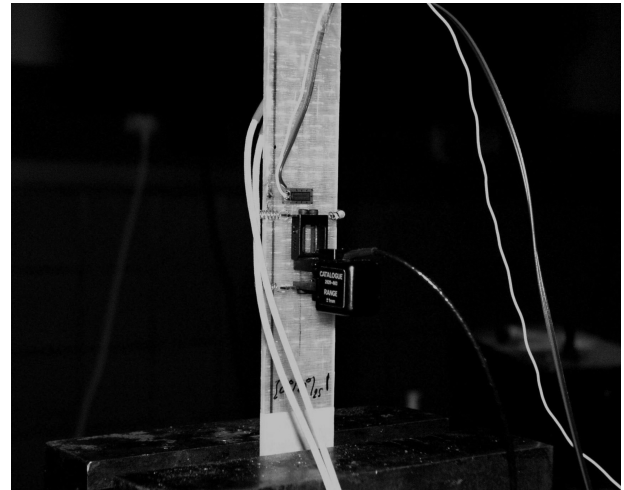


Fig. 8 Instrumentation of the  $[0^\circ/90^\circ]_{2s}$  glass/epoxy specimens.

value must be stress dependent because no further damage occurs during unloading.

#### MEASUREMENTS OF $\nu_{xy}$ UNDER FATIGUE LOADING

In order to assess the sensitivity of the Poisson's ratio  $\nu_{xy}$  for fatigue damage, tension–tension fatigue tests have been conducted on the same material. The specimen geometry was the same as shown in Fig. 1, but the longitudinal strain gauge has been replaced by an extensometer. The fatigue tests were strain-controlled, so that the measurement of the transverse strain  $\epsilon_{yy}$  immediately yields the value of the Poisson's ratio  $\nu_{xy}$ .

The maximum strain level was chosen 0.006 (0.6%), because this strain level is slightly higher than the knee-point in the static stress–strain curve (see Fig. 2). Using a 'strain ratio'  $R$  of 0.1 (similar to the stress ratio in fatigue), the minimum strain level is 0.0006 (0.06%).

The fatigue tests were done at 2 Hz on an Instron servohydraulic testing machine.

Figure 8 shows the clamped specimen with its instrumentation. The extensometer measures the longitudinal strain, the transverse strain gauge measures the transverse strain and a thermocouple monitors the surface temperature of the composite laminate. Load and displacement were measured by the servohydraulic machine control.

Normally, the life time of strain gauges in fatigue is very limited, because the limit strain levels they can endure in fatigue, are very much reduced compared to static operation. However, in this case the transverse strain levels were very small (a few hundred microstrains) and no temperature rise of the surface was detected from the thermocouple.

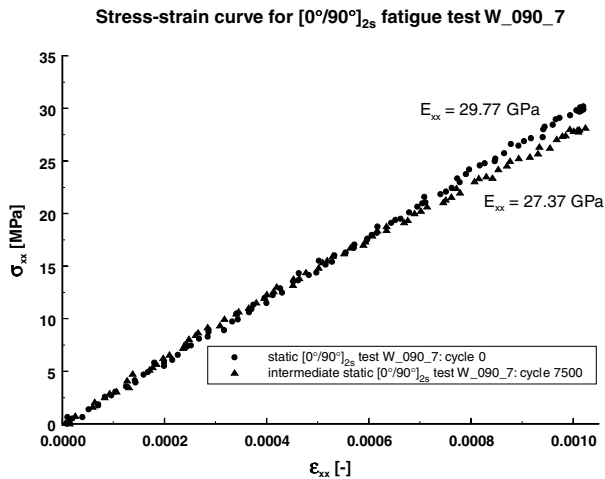


Fig. 9 Stress–strain curve for the initial and intermediate static tensile tests of the  $[0^\circ/90^\circ]_{2s}$  fatigue test W\_090\_7.

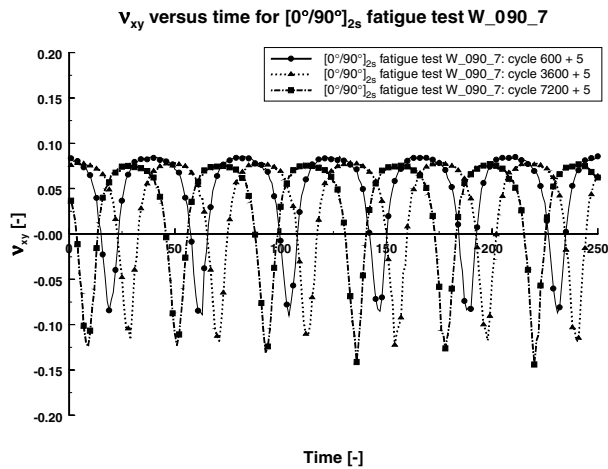


Fig. 10 Time history of the Poisson's ratio  $\nu_{xy}$  for the  $[0^\circ/90^\circ]_{2s}$  specimen W\_090\_7 at three chosen intervals in the fatigue test.

The signals of load, displacement, extensometer, strain gauge and temperature were each sampled at 100 Hz every 5 min for five subsequent loading cycles with a National Instruments NI DAQPAD–6052E measurement card and LabVIEW software.

For the first fatigue test W\_090\_7, 7500 loading cycles were applied. The stress–strain curve was measured before fatigue testing, but only to a very low axial strain of 0.001 (0.1%), because the failure strain of the  $90^\circ$  plies is only 0.0025 (0.25%) (see Table 2). After stopping the fatigue test, the same static tensile test was repeated. Figure 9 shows the measured static stress–strain curves for cycle 0 and cycle 7500. A degradation of the axial stiffness  $E_{xx}$  is observed from 29.77 to 27.37 GPa.

Figure 10 shows the time history of the Poisson's ratio  $\nu_{xy}$  at three chosen intervals in the fatigue test. The ab-

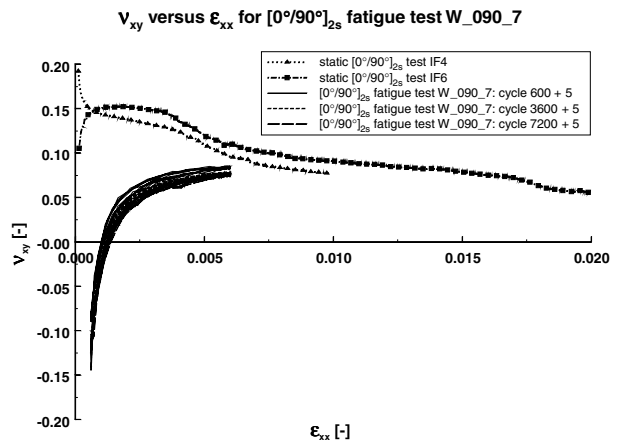


Fig. 11 Evolution of the Poisson's ratio  $\nu_{xy}$  in function of the longitudinal strain  $\epsilon_{xx}$  for the  $[0^\circ/90^\circ]_{2s}$  specimen W\_090\_7 at three chosen intervals in the fatigue test.

scissa shows the sample number of the data acquisition (proportional with time). Five full cycles correspond with 2.5 s (2 Hz). The behaviour is very similar with that in cyclic loading–unloading tests (see Fig. 6).

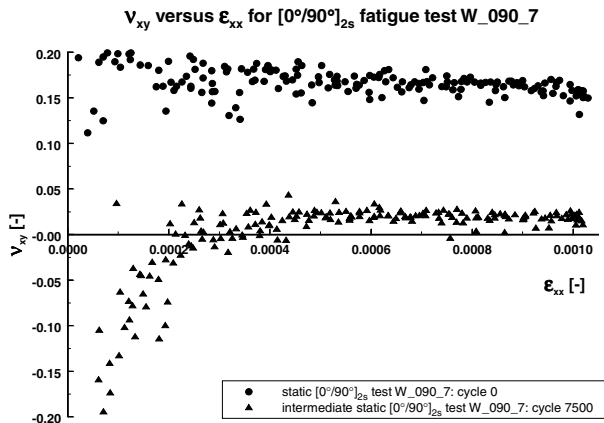
The maximum value of the Poisson's ratio  $\nu_{xy}$  is clearly decreasing with increasing loading cycles, while the negative peaks are increasing as well.

In Fig. 11, the evolution of the Poisson's ratio  $\nu_{xy}$  is again plotted against the longitudinal strain  $\epsilon_{xx}$  for the same sets of five cycles as shown in Fig. 10. The shape of the loading–unloading curves is very similar to the one showed in Fig. 7. It must be noticed as well that the Poisson's ratio shows a sharp decline during the first loading cycles. After only 600 cycles, the value has already decreased considerably.

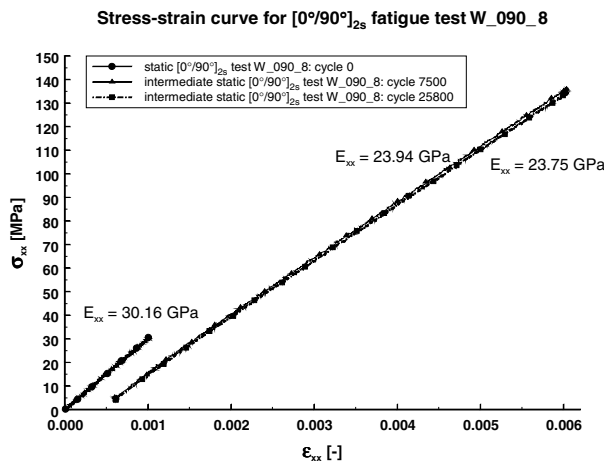
To be sure that the shape of the  $\nu_{xy}$ – $\epsilon_{xx}$  curves is not due to strain rate effects, the evolution of the Poisson's ratio  $\nu_{xy}$  is plotted against the longitudinal strain  $\epsilon_{xx}$  for the static tensile tests that were done before the fatigue testing and after 7500 cycles.

Figure 12 shows that the initial Poisson's ratio  $\nu_{xy}$  is about 0.16 [–], while after 7500 cycles, the shape of the  $\nu_{xy}$ – $\epsilon_{xx}$  curve appears again. It is important to stress the fact that the maximum applied strain  $\epsilon_{xx}$  during these static tensile tests was only 0.001 (0.1%), in order to be sure that no damage was introduced into the specimen before fatigue testing. Indeed, this strain level is well below the transverse failure strain of the  $90^\circ$  plies (0.0025, see Table 2).

For the second fatigue test W\_090\_8, 40 000 loading cycles were applied. The stress–strain curve was measured before fatigue testing, but again only up till a very low axial strain of 0.001 (0.1%). At two intermediate loading cycles, the fatigue test was stopped and the same static tensile test was repeated.



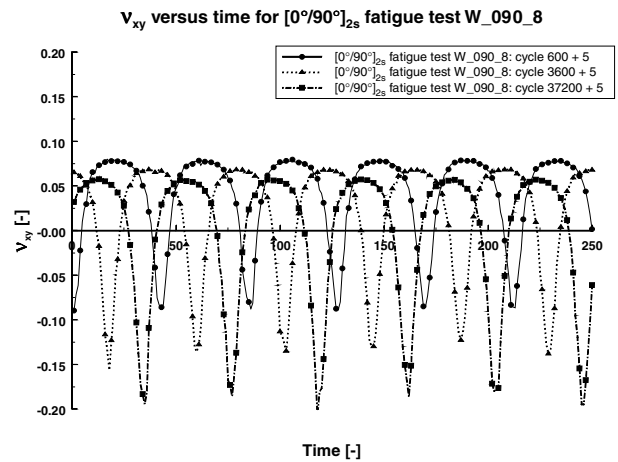
**Fig. 12** Evolution of the Poisson's ratio  $\nu_{xy}$  in function of the longitudinal strain  $\epsilon_{xx}$  for the initial and intermediate static tensile tests of the  $[0^\circ/90^\circ]_{2s}$  fatigue test W\_090\_7.



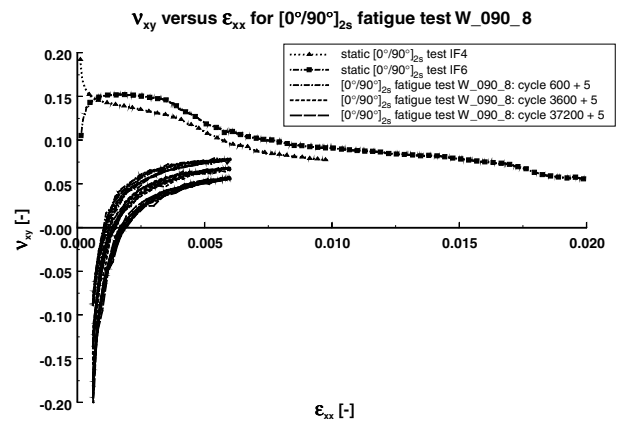
**Fig. 13** Stress–strain curve for the initial and intermediate static tensile tests of the  $[0^\circ/90^\circ]_{2s}$  fatigue test W\_090\_8.

Figure 13 shows the stress–strain curves before fatigue testing, and at cycle 7500 and cycle 25 800. The initial stiffness of 30.16 GPa decreases to 23.94 GPa, and further to 23.75 GPa. The comparison of the stiffness degradations in Fig. 13 and Fig. 9 is not straightforward due to the very different strain scale. In Fig. 13 a least-squares linear fit to the full strain range [0.0006–0.006] has been done. If only the strain interval [0.0006–0.001] is used for determination of the Young's modulus, the values are 26.92 and 26.43 GPa, respectively.

Figure 14 shows the time history of the Poisson's ratio  $\nu_{xy}$  for three chosen intervals in the fatigue test. The abscis shows again the sample number of the data acquisition, but the five plotted cycles correspond again with 2.5 s (2 Hz). The behaviour is very similar with that in cyclic loading-unloading tests (see Fig. 7).



**Fig. 14** Time history of the Poisson's ratio  $\nu_{xy}$  for the  $[0^\circ/90^\circ]_{2s}$  specimen W\_090\_8 at three chosen intervals in the fatigue test.



**Fig. 15** Evolution of the Poisson's ratio  $\nu_{xy}$  in function of the longitudinal strain  $\epsilon_{xx}$  for the  $[0^\circ/90^\circ]_{2s}$  specimen W\_090\_8 at three chosen intervals in the fatigue test.

In Fig. 15, the evolution of the Poisson's ratio  $\nu_{xy}$  is again plotted against the longitudinal strain  $\epsilon_{xx}$  for the same sets of five cycles as shown in Fig. 14. The correspondence with Fig. 11 is again very good. It seems that both the maximum and minimum value of the Poisson's ratio are affected by the fatigue damage and could be a usable damage variable.

Here again, the evolution of the Poisson's ratio  $\nu_{xy}$  versus longitudinal strain  $\epsilon_{xx}$  was measured under static loading conditions as well, to eliminate strain rate effects. However, the intermediate static tests were now performed up to a maximum strain of 0.006 (0.6%), as opposed to Fig. 12.

Figure 16 shows that the initial Poisson's ratio  $\nu_{xy}$  is now about 0.15 [–]. The scatter is quite large in the initial strain regime, due to the very low axial strains  $\epsilon_{xx}$  and even lower transverse strains  $\epsilon_{yy}$ . However, at an axial strain  $\epsilon_{xx}$  of

0.001, the Poisson's ratio converges to a more or less constant value. In the intermediate static tests at cycles 7500 and 22 800, the same strain range [0.0006–0.006] as in the fatigue loading cycles has been applied. The same shape of the  $\nu_{xy}-\epsilon_{xx}$  curve appears.

More fatigue tests have been done that confirm the behaviour discussed above. Finally, some tests were taken up till final failure. The glass/epoxy composite is fully cracked then and turns white. After 135 000 cycles failure occurs by fracture of the fibres.

The typical damage patterns are shown in Fig. 17 for 133 000 cycles (left) and at failure (135 000 cycles).

In this stage of severe damage, the evolution of the Poisson's ratio  $\nu_{xy}$  versus longitudinal strain  $\epsilon_{xx}$  still shows the same shape, but the amplitude is about 10 times smaller, as shown in Fig. 18. Some precaution is also necessary in this case. Due to the damaged surface, the bonding quality of the transverse strain

gauge will have deteriorated, so that the strain transfer from the composite surface to the strain gauge is not reliable anymore. Perhaps a biaxial extensometer could be used to solve this problem.

However, as the same shape still appears, it can be assumed that the measurements are still valid.

### CONCLUSIONS

It has been demonstrated that both the amplitude and shape of the  $\nu_{xy}-\epsilon_{xx}$  curve change when damage is present in a composite laminate. The static evolution of the Poisson's ratio is the envelope that encloses the cyclic  $\nu_{xy}-\epsilon_{xx}$  curves. Also, the degradation of the Poisson's ratio is much larger than that of the stiffness.

Further research is required to investigate the value of using the Poisson's ratio as a damage indicator for other material combinations than glass/epoxy.

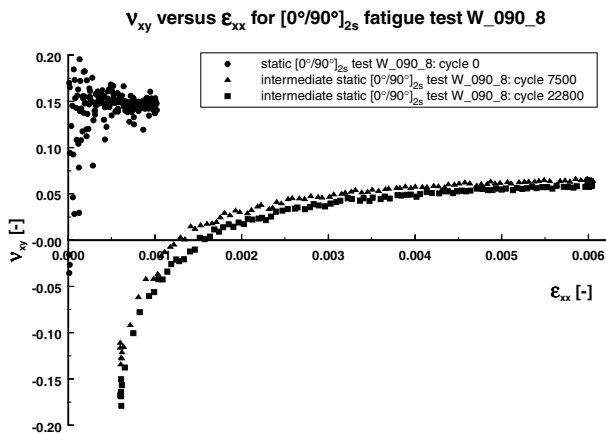


Fig. 16 Evolution of the Poisson's ratio  $\nu_{xy}$  in function of the longitudinal strain  $\epsilon_{xx}$  for the initial and intermediate static tensile tests of the  $[0^\circ/90^\circ]_{2s}$  fatigue test W\_090.8.

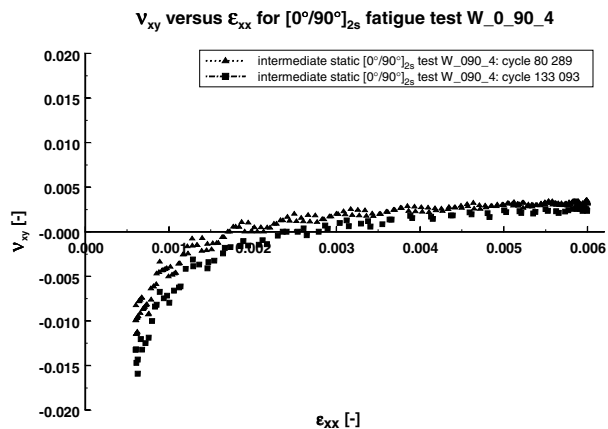


Fig. 18 Evolution of the Poisson's ratio  $\nu_{xy}$  in function of the longitudinal strain  $\epsilon_{xx}$  for the intermediate static tensile tests of the  $[0^\circ/90^\circ]_{2s}$  fatigue test W\_090.4.

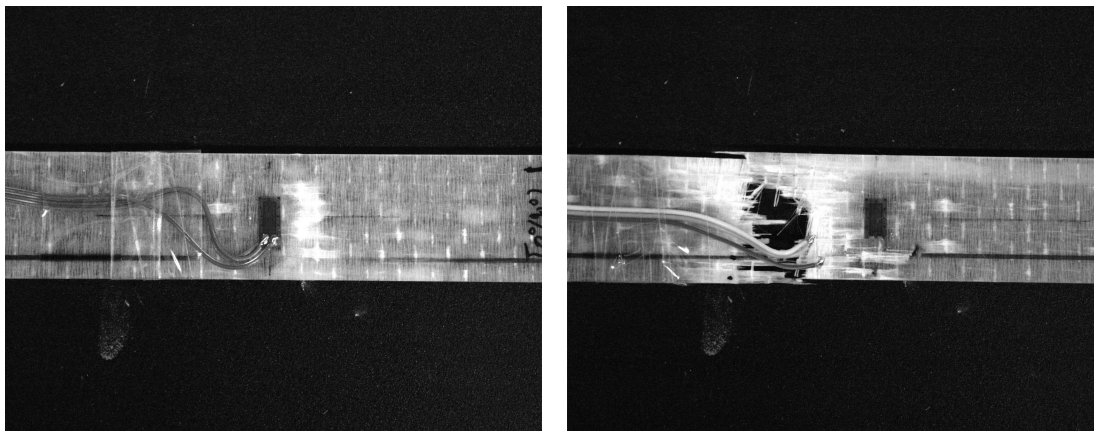


Fig. 17 Typical damage patterns in the  $[0^\circ/90^\circ]_{2s}$  specimens (a) close to failure, and (b) after failure.

## Acknowledgements

The author W. V. P. gratefully acknowledges his finance through a grant of the Fund for Scientific Research – Flanders (F.W.O.) Proceedings on CD-ROM. The authors also express their gratitude to Syncoglas for their support and technical collaboration.

## REFERENCES

- 1 Mallick, P. K. (1997) *Composites Engineering Handbook*. Marcel Dekker Inc., New York.
- 2 Herakovich, C. T. (1998) *Mechanics of Fibrous Composites*. John Wiley & Sons, Inc., New York.
- 3 Schulte, K., Baron, Ch., Neubert, H., et al (1985) Damage development in carbon fibre epoxy laminates : Cyclic loading. In : *Proceedings of the MRS-symposium "Advanced Materials for Transport", November 1985*, Strassbourg, pp. 8.
- 4 Schulte, K., Reese, E. and Chou, T.-W. (1987) Fatigue behaviour and damage development in woven fabric and hybrid fabric composites. In : *Sixth International Conference on Composite Materials (ICCM-VI) & Second European Conference on Composite Materials (ECCM-II)* (Edited by F. L. Matthews, N. C. R. Buskell, J. M. Hodgkinson, and J. Morton) **Vol. 4**. Proceedings, 20–24 July 1987, Elsevier, London, UK, pp. 4.89–4.99.
- 5 Schulte, K. (1984) Stiffness reduction and development of longitudinal cracks during fatigue loading of composite laminates. In : *Mechanical characterisation of load bearing fibre composite laminates. Proceedings of the European Mechanics Colloquium 182, 29–31 August 1984, Brussels*, (Edited by A. H. Cardon and G. Verchery) Elsevier, Belgium, pp. 36–54.
- 6 Fujii, T., Amijima, S. and Okubo, K. (1993) Microscopic fatigue processes in a plain-weave glass-fibre composite. *Comp. Sci. Technol.* **49**, 327–333.
- 7 Pandita, S. D., Huysmans, G., Wevers, M. and Verpoest, I. (2000) Tensile fatigue behaviour of glass-plain weave fabric composites in the on and off-axis directions. *Proceedings of the Fifth International Conference on Textile Composites*, Leuven, Belgium, 18–20 September 2000.
- 8 Sidoroff, F. and Subagio, B. (1987) Fatigue damage modelling of composite materials from bending tests. In : *Sixth International Conference on Composite Materials (ICCM-VI) & Second European Conference on Composite Materials (ECCM-II)* (Edited by F. L. Matthews, N. C. R. Buskell, J. M. Hodgkinson, and J. Morton) **Vol. 4**. Proceedings, 20–24 July 1987, Elsevier, London, UK, pp. 4.32–4.39.
- 9 Vieilleigne, S., Jeulin, D., Renard, J. and Sicot, N. (1997) Modelling of the fatigue behaviour of a unidirectional glass epoxy composite submitted to fatigue loadings. In: *International Conference on fatigue of composites* (Edited by S. Degallaix, C. Bathias and R. Fougères). Proceedings, 3–5 June 1997, La Société Française de Métallurgie et de Matériaux, Paris, France, pp. 424–430.
- 10 Kawai, M. (1999) Damage mechanics model for off-axis fatigue behavior of unidirectional carbon fiber-reinforced composites at room and high temperatures. In: *Proceedings of the Twelfth International Conference on Composite Materials (ICCM-12)* (Edited by T. Massard and A. Vautrin). Paris, France, 5–9 July 1999, pp. 322.
- 11 Hwang, W. and Han, K. S. (1986) Fatigue of composites - Fatigue modulus concept and life prediction. *J. Comp. Mater.* **20**, 154–165.
- 12 Hwang, W. and Han, K. S. (1986) Cumulative damage models and multi-stress fatigue life prediction. *J. Comp. Mater.* **20**, 125–153.
- 13 Whitworth, H. A. (1987) Modelling stiffness reduction of graphite epoxy composite laminates. *J. Comp. Mater.* **21**, 362–372.
- 14 Yang, J. N., Jones, D. L., Yang, S. H. and Meskini, A. (1990) A stiffness degradation model for graphite/epoxy laminates. *J. Comp. Mater.* **24**, 753–769.
- 15 Brøndsted, P., Andersen, S. I. and Lilholt, H. (1997) Fatigue damage accumulation and lifetime prediction of GFRP materials under block loading and stochastic loading. In : *Polymeric Composites - Expanding the Limits. Proceedings of the 18th Risø International Symposium on Materials Science, 1–5 September 1997* (Edited by S. I. Andersen, P. Brøndsted, H. Lilholt, Aa. Lystrup, J. T. Rheinländer, B. F. Sørensen and H. Toftegaard). Risø International Laboratory, Roskilde, Denmark, pp. 269–278.
- 16 Brøndsted, P., Lilholt, H. and Andersen, S. I. (1997) Fatigue damage prediction by measurements of the stiffness degradation in polymer matrix composites. In : *International Conference on fatigue of composites* (Edited by S. Degallaix, C. Bathias and R. Fougères) Proceedings, 3–5 June 1997, La Société Française de Métallurgie et de Matériaux, Paris, France, pp. 370–377.
- 17 Bando, S., Matsumura, K., Zako, M., Shiino, T. and Kurashiki, T. (2001) On the detection of fatigue damage in CFRP by measuring Poisson's ratio. In: *Eighth International Conference on Composites Engineering (ICCE/8)* (Edited by D. Hui) Proceedings. Tenerife, Spain, 5–11 August 2001, pp. 55–56.
- 18 Pidaparti, R. M. and Vogt, A. (2002) Experimental investigation of Poisson's ratio as a damage parameter for bone fatigue. *J. Biomed. Mater. Res. Part A* **59**, 282–287.
- 19 Sol, H. and de Wilde, W. P. (1988) Identification of elastic properties of composite materials using resonant frequencies. In : *Proceedings of the International Conference "Computer Aided Design in Composite Material Technology"* (Edited by C.A. Brebbia, W. P. de Wilde and W. R. Blain) 1988, Springer-Verlag, Southampton, pp. 273–280.
- 20 Sol, H. (1990) Identification of the complex moduli of composite materials by a mixed numerical/experimental method. In : *Proceedings of the second International Conference on Computer Aided Design in Composite Material Technology* (Edited by W. P. de Wilde and W. R. Blain) 25–27 April 1990, Springer-Verlag, Brussels, pp. 267–279.
- 21 Van Paeppegem, W., De Baere, I. and Degrieck, J. (2005) Modelling the nonlinear shear stress-strain response of glass fibre-reinforced composites. Part I: Experimental results. *Comp. Sci. Technol.* **66**, 1455–1464.
- 22 Van Paeppegem, W., De Baere, I. and Degrieck, J. (2005) Modelling the nonlinear shear stress-strain response of glass fibre-reinforced composites. Part II: Model development and finite element simulations. *Comp. Sci. Technol.* **66**, 1465–1478.